Metrol. Meas. Syst., Vol. 30 (2023) No. 4, pp. 637–654
DOI: 10.24425/mms.2023.147951

PAN POLSKA AKADEMIA NAUK

METROLOGY AND MEASUREMENT SYSTEMS
Index 330930, ISSN 0860-8229
www.metrology.wat.edu.pl

M&MS

HYPERSPECTRAL IMAGING – A SHORT REVIEW OF METHODS AND APPLICATIONS

Jędrzej Kowalewski[1,2)], Jarosław Domaradzki[2)], Michał Zięba[1)], Mikołaj Podgórski[1,2)]

1) Scanway, Duńska 9, 54-427 Wrocław, Poland (✉ *j.kowalewski@scanway.pl, m.zieba@scanway.pl, m.podgorski@scanway.pl*)
2) Wrocław University of Science and Technology, Faculty of Electronics, Photonics and Microsystems, Janiszewskiego 11/17, 50-372 Wrocław, Poland (*jaroslaw.domaradzki@pwr.edu.pl*)

Abstract

This paper takes a look at the state-of-the-art solutions in the field of spectral imaging systems by way of application examples. It is based on a comparison of currently used systems and the challenges they face, especially in the field of high-altitude imaging and satellite imaging, are discussed. Based on our own experience, an example of hyperspectral data processing is presented. The article also discusses how modern algorithms can help in understanding the data that such images can provide.

Keywords: hyperspectral imaging, spectral imaging, observation methods, infrared detector.

1. Introduction

Any process in science and technology, the purpose of which is to study an object or phenomenon, involves taking appropriate steps and using appropriate measurement tools. The vast majority of such processes are based on one-dimensional measurements, *i.e.*, those in which, under specific conditions (*e.g.* at a specific location), a single physical quantity is observed. The reason for such one-dimensional (point) observation is to simplify the architecture of measurement equipment and techniques. A simple example could be the measurement of surface water temperature of the ocean which can be realized with a single sensor that provides temperature information only at selected point on the water's surface. In many different applications such point measurements are sufficient. However, if it is important for the research process to determine the temperature at multiple locations at the same time, it will be necessary to use the so-called imaging techniques.

Article history: received April 17, 2023; revised July 6, 2023; accepted July 10, 2023; available online November 16, 2023.

Imaging, from the technical point of view, can be defined as the acquisition and representation of point measurement data in the spatial domain [1]. In the simplest case, individual point's data are stored in the cells of a two-dimensional matrix at locations that correspond to their actual arrangement in space – these are called pixels. Sets of such pixels are referred to as images. Such recording allows reconstruction of images in grayscale. In the case of the most common imaging in the form of tri-color images, we deal with a set of three such matrices with each matrix corresponding to a different component color (R, G and B).

Another technique, commonly used nowadays not only in scientific laboratories, is spectroscopy (or spectrophotometry). This technique, based on the analysis of the spectrum of light in the wavelength (or frequency) domain, makes it possible to analyze, among the others, the material composition of substances under analysis. Information is obtained due to the interaction of light with matter (through reflection or absorption) and is its fingerprint, that allows to recognize its chemical composition [2].

The combination of the imaging technique and spectroscopy is referred to as imaging spectrometry, also known today as multi- or hyper-spectral imaging [2, 3]. Numerical data of each image pixel is stored in a three-dimensional matrix in which the third dimension is related to the wavelength of optical radiation.

The formal definition of hyperspectral imaging, after Qian [2], is "the acquisition of many images of contiguous, narrow, registered spectral bands such that for each pixel a radiance spectrum can be derived". The difference between "hyper-" and "multi-" spectral imaging is that in multispectral imaging systems we may distinguish only a limited number of wide spectral bands separated by (blind) gaps. The number of channels in hyperspectral imaging can be counted the hundreds, but even more important is the bandwidth that in this case is typically 10 nm or even less, whereas for multispectral systems the bandwidth of selected several bands is typically about 100 nm.

Simultaneous recording and analyzing images in a very large number of relatively narrow spectral ranges (including those invisible to the human eye, such as infrared) opens up new possibilities, as it allows the world to be seen in an enhanced form, without simplifying or losing information. The invention of hyperspectral imaging is another step toward increasing the resolution of imaging in the light spectrum domain. This invention can be compared to the digital revolution in imaging, which was sparked by the invention of the CCD (*charge coupled device*) sensors and their replacement of traditional analog film. Currently, spectral imaging has emerged as a new, fascinating generation of remote sensing for application in a broad range of fields of earth observation starting from the military and defense, geology, biology, environment, atmosphere, climate, agriculture, mining and other purposes [2–6]. At present, hyperspectral imaging systems, mainly due to their relatively high price, are only used to a limited extent. However, it is anticipated that the spread of such techniques into even wider and more everyday applications is only a matter of time.

In this article, selected spectral imaging systems are used as application examples; they have been selected and reviewed based on the authors' recent experience. By comparing currently used spectral imagers, a general overview of the challenges is highlighted, especially in the field of high-altitude and satellite imagery. The last group is crucial for modern hyperspectral data acquisition, and the paper presented brings the state-of-art solutions in this field. This article also introduces digital hyperspectral image processing, and how modern algorithms can help understand the data that such images can provide.

2. Review of spectral imaging missions and systems

This chapter contains a short review on the history of satellite missions using spectral imaging instrumentation, and an overview of primary elements of each spectral imaging system with a special focus on cameras.

2.1. Airborne hyperspectral imaging

One of the very first steps into hyperspectral imaging, different than astronomy, were airborne platforms and agriculture related observations. As early as 1966, Michigan University of Technology started to adapt military imaging instruments for civil applications. The university started an imaging campaign registering from 12 to 18 spectral channels for instructional purposes. Several years later, between 1970–75, the Department of Agriculture ordered an imaging campaign to obtain data which could show patterns in the spread of corn disease epidemy called SCLB (*Southern Corn Leaf Blight*). The following imaging runs resulted in considerable amounts of data which remain important sources of data even today, especially in the context of types of soil, crops, state of biomass and invasive species in agriculture. This campaign together with the Landsat mission were turning points in the imaging technology development and showed the full potential of spectral imaging [7].

The next important airborne spectral imaging application and instrument was AVRIS (*Airborne Visible/InfraRed Imaging Spectrometer*), developed by NASA JPL. First implementation of AVRIS was in 1987 and its maiden flight was completed onboard NASA ER-2 with data obtained at the altitude of 20 km above the ground. The quality and radiometric correlation are considered as the best hyperspectral implementation of remote sensing in Earth Observation [8].

Other important airborne hyperspectral implementations are commercial products such as DAIS (*Digital Airborne Imaging Spectrometer*) developed by GERoM (*Geophysical Environmental Research of Millbrook*) in 1987, CASI (*Compact Airborne Spectrographic Imager*) from ITRES (1989) and HYDICE (*HYperspectral Digital Imagery Collection Experiment*) from NRL (*Naval Research Lab*) from 1994. The spectrally very similar HyMap instrument from HyVista Corporation was introduced in 1999 [8].

2.2. Satellite missions with hyperspectral imaging instruments on-board

The first spectral remote imaging systems (multispectral) appeared as early as the 1970s with the satellite Landsat mission (launched in 1972). Since then, many missions with on-board spectral imaging systems have been launched, with activity peaking in the 1980s and 1990s. However, it seems that a tremendous amount of application of (hyper)spectral imaging has begun with the new millennium. From a literature review, one can see a rapid increase in the number of publications on the subject of hyperspectral remote sensing, and especially after 2010, it has increased nearly three times year-on-year [4]. The particular factors that influenced this accelerated evolution was the development of semiconductor technology and computing techniques as well as the initiation of low-cost space missions by private corporations with the use of cubsats [3]. Table 1 presents an overview of selected satellite missions with on-board hyperspectral instruments together with their base imaging parameters, launched (or yet planned) in the last years.

Spectral imaging is most often used to image electromagnetic radiation in bands ranging from ultraviolet (UV), through the visible (VIS) range, to infrared (usually SWIR – *short wave infrared*). However, there are also some examples of exploration of the far infrared range, up to about 15 μm, as in MetOP-OG or MODIS missions (Table 1).

Table 1. Satellite missions and instruments using hyperspectral imaging instruments [9–25].

Mission/Instrument Name	Agency/Country	Spectral Range [µm]	No. of Channels	Ground Sampling Distance – GSD [m]	Launching Year	Ref.
MODIS	NASA	0.460–14.390	36	250–1 000	1999 2002	[9]
EO–1	NASA	0.357–2.570	242	30	2000	[10]
PROBA–1	ESA	0.415–1.050	63/150	18	2001	[11]
ADEOS-II	Japan	0.380–12.00	36	1 000	2002	[12]
IMS–1	India	0.400–0.950	64	505	2008	[13]
HysIS	India	0.400–2.400	316	30	2018	[14]
PRISMA	ASI – Italy	0.400–2.500	250	30	2019	[15]
Jilin–1	China	–	28	5	2019	[16]
HISUI	Japan	0.400–2.500	185	30	2020	[17]
GEO-KOMPSAT-2B	Korea	0.300–0.500	250	7 000	2020	[18]
EOS-3 (GISAT-1)	India	0.900–2.500	150	200	2021	[19]
EnMap	DLR – Germany	0.420–2.450	228	30	2022	[20]
TEMPO	NASA	0.290–0.740	666	4 400	2022	[21]
Intuition-One	Poland	0.470–0.900	150	25	2023	[22]
HyspIRI	USA	0.380–2.510	–	60	2024	[23]
MetOP-SG A1 MetOP-SG A2 MetOP-SG A3 (UVNS)	ESA	0.270–2.385	3936	7 000–28 000	2024	[24]
MTG-S1 MTG-s2 (UVN)	ESA	0.305–0.775	598	8 000	2024	[24]
FLEX	ESA	0.500–0.780	300	300	2024	[25]

2.3. Elements of spectral imaging system

Imaging systems typically consist of an optical system, a camera and data processing unit. Depending on the required spectral range, different types of sensors are used. For example, for VIS and near-UV silicon detectors are suitable for which the range of spectral sensitivity is, at most, from 400 nm to 1100 nm. For SWIR, it is necessary to use detectors that are sensitive in this spectral range, such as those based on InGaAs, which allow recording of spectra typically from about 700 nm to 1700 nm. Table 2 provides an overview of commercially available detectors used in spectral imaging systems.

The data presented in Table 2 shows a wide variety of available detectors in terms of both available spectral ranges and technology from which they are made. The role of the sensor is to convert an optical signal (electromagnetic radiation in the range of optical waves) to an electric one. Conversion takes place at each particular pixel of a 2-dimensional sensor's matrix, giving the possibility of recording the image presented to the sensor. CCD detectors were introduced to imaging systems as early as the 1970s. Unlike CCD detectors, the CMOS (*Complementary Metal Oxide Semiconductor*) technology came into widespread use in the 1990s and now occupies most

Table 2. Review of cameras used in spectral imaging. FOV – field of view [26–38].

Manufacturer	Model	Sensor Technology	Resolution [Mpx]	FOV [deg]	Spectral Range [nm]	No. of Channels	Frame Rate [Hz]	Weight [kg]	Ref.
CORNING	microHSI 410	CCD/CMOS hybrid	–	29.5	400–1000	–	300	0.45	[26]
CUBERT	ultris x20 plus	–	3	35	350–100	164	6	0.63	[27]
ELDIM	EZLITE HXS	Cooled CCD	3	±60	400–700	15(VIS) + 2(NIR)	–	10.00	[28]
EVK	HELIOS EQ32	–	320px	–	900–1700	8	446	7.80	[29]
Scanway	HSS-1020	CMOS	1	–	400–1100	2000	–	9.0	[30]
GAMAYA		Sensor OXI	2		450–630 600–950 450–950 600–950	16, 25, 40, 100	16–30	0.10	[30]
HINDSIGHT	SpecVu	CMOS	2.3	6–22	400–1000	600	–	2.00	[30]
HySpex	VNIR-1800	CMOS		17	400–1000	186	260	5.00	[31]
	VNIR-3000N	–	–	16	400–1000	300	117	5.00	
	VS-1200	–	–	40	400–1000	400	285	35	
	SWIR-640	–	–	16	960–2500	360	140	4.10	
	Mjolnir VS-620	–	–	20	400–2500	490	285(VIS) 100(NIR)	6.00	
	Baldur V-1024 N	–	–	16/40	400–1000	72/88	–	–	
IMEC	SNAPSCAN SWIR	–	0.8	–	1100–1650	100	–	0.895	[32]
	SNAPSCAN VNIR	–	7	–	470–900	150	–	0.58	
	SNAPSHOT UAV VIS+NIR	–	1	–	480–860	25	50	0.50	
	Custom	–	–	–	–	–	–	–	

Metrol. Meas. Syst., Vol. 30 (2023), No. 4, pp. 637–654
DOI: 10.24425/mms.2023.147951

Table 2 continued.

Manufacturer	Model	Sensor Technology	Resolution [Mpx]	FOV [deg]	Spectral Range [nm]	No. of Channels	Frame Rate [Hz]	Weight [kg]	Ref.
INNO-SPEC	RedEye 1.7	–	0.08	–	950–1700	up to 66	330	4.30	[33]
	RedEye 2.2	–	0.08	–	1200–2200	up to 66	330	10.50	
	Blueeye	CMOS	4	–	220–380	–	40	1.30	
	Greeneye	CMOS	1	–	400-1000	–	54	2.00	
JAI	Fusion Series		2	–	405–1000	3 (VIS) 1 (NIR)	200	–	[34]
LLA instruments	uniSPEC0.9HSI	CMOS	–	–	395–995	–	11–500	16.80	[35]
	KUSTA1.7 MSI	InGaAs	–	–	950-1700	–	270		
	KUSTA1.9 MSI		–	–	1320–1900	–	795		
	Kusta2.2 MSI		–	–	1620–2190	–	795		
MicaSense	Dual Camera System		3.6	47	475–740	10	–	0.508	[36]
Ocean Insight-FluxData	FD-1665	CCD	1	–	400–1100	3–8	70	–	[37]
SPECIM	FX50	InSb	–	24, 45, 60	2700–5300	154	380	7	[38]
	FX-10		1	40	400–1000	220	> 330	1.4	
	FX-17	InGaAs		40	900–1700	230	> 670	1.4	
	IQ	–	–	–	400–1000	–	–	–	
	LWIR	–	–	–	8000–12000	42/84	–	3.50/13.10	

of the market for commercial imaging detectors, including amateur photography or special, *e.g.*, military applications. These detectors have the advantage of higher frame rates, lower power requirements and much simpler manufacturing technology compared to CCD detectors. Overall classification of hyperspectral cameras comes from its planned application. A general tradeoff is the spectral (number of channels) vs spatial resolution (number of pixels) which is directly connected with the acquisition technique used in a particular application. For most common areas, such as agriculture, mining classification and food sorting, a linescan camera with the number of spectral channels not greater than 100, and spatial resolution not greater than 3 million of pixels can be used. It is plausible to assume that instruments with greater spectral and spatial resolutions are aimed at highly demanding applications and platforms such as airborne, orbital or military imaging.

Independent of the type of sensor used, imaging in a wide spectrum of wavelengths requires appropriate segmentation of the detected optical radiation to discrete (or continuous) wave bands of the desired width. The most commonly used techniques are the following:

- diffraction grating – used to split the light, which is then directed to the sensor surface. The use of a 2D matrix of active pixels in combination with a diffraction grating makes it possible to obtain a linear spectral imaging sensor,
- prism – used to split the light beam. In a similar way to the diffraction grating-based sensors, it is possible to obtain linear hyperspectral imaging sensors,
- spectral filters placed in front of the sensor. A plate with applied bandpass filters is placed directly in front of the sensor surface in such a way as to separate groups of pixels responsible for imaging in particular spectral bands. This allows the construction of a spectral imaging device in a spatial-spectral configuration (imaging is performed in the field mode, but to obtain a full spectral image of the subject, it requires relative movement of the imaging platform to the to the subject),
- spectral filters applied directly to the sensor's surface. A separate Fabry-Pérot filter is applied directly to each imaging pixel. Technologies that allow filters to be applied directly to the pixel's surface are currently the subject of intensive work by the world's leading companies and research institutes, and sensors based on their use are finding increasing use in observational instruments. The methodology for developing sensors using this technology allows for unrestricted shaping of both geometry and distribution of spectral bands within the sensor as well as unrestricted shaping of the spectral characteristics of a given pixel.

Another interesting proposition is the application of an acousto-optic tunable filter utilizing a birefringent crystal and piezoelectric transducer excited with a radio-frequency signal [39].

Because the entire spectrum is acquired for each pixel of a camera sensor, hyperspectral images contain a huge number of data (sometimes referred as hypercubes). Extraction of desired information requires further processing of collected data using different algorithms that require high computing power.

2.4. Additional special systems requirements

Athermicity. A fundamental problem for spectral imaging systems operating on satellite missions is to ensure athermicity, *i.e.*, minimized susceptibility to temperature fluctuations. Regardless of the band at which a hyperspectral system operates, temperature has a significant impact on the behavior of the optical instrument. The basic phenomena, related to thermality, are the deformation, shortening and elongation of components with temperature change. If the instrument operates in the VIS and SWIR bands, the problems are purely mechanical, while in the case of the deeper infrared bands (above 2 μm of wavelength), the increased temperature turns the

lenses and mirrors of the optical system into objects that emit the light seen by the sensor. Thus, it becomes clear that the basic requirement for an instrument used on aerospace platforms is to choose a design that ensures the optical path independent of temperature deformation phenomena, and to decide whether active cooling (less often heating) of optical system components is needed.

Vibrations. High levels and specific vibration characteristics are the hallmarks of aircraft and space platforms. The system adapted for use on such platforms must be designed to resist vibrations that may cause undesirable disassembly of its components, decalibration or even damage. Most often this is done through the use of properly selected vibro-isolators, and if such a solution is not possible, because of $e.g.$ limited weight – the implementation of adhesives to the final, inseparable joining of the instrument's elements.

Power consumption. Due to limited power supply, which is extremely prominent in space platforms, spectral instruments must be characterized by low power consumption and overall low energy requirements during a mission or operation. This is an extremely difficult requirement because of very frequent use of FPGAs which have high capabilities and flexibility in data processing but require relatively high power and efficient heat dissipation or cooling.

Spectral resolution and sensitivity. Due to the long imaging distance, which is a feature of aircraft and space missions, imaging instruments using these platforms must have high resolution capabilities and high radiometric sensitivity. Currently, a race is underway in the space sector whose the aim is to achieve the highest possible resolution from the smallest optical instrument possible. An additional difficulty is that the resolution depends on the sensitivity of the system and, in the case of hyperspectral instruments, when the photon intensity is too low, individual pixels receive residual photons. This is due to the division of the visible spectrum into many spectral channels which divides the number of photons into individual channels. For example, a panchromatic instrument, that is, imaging with broad spectral bands, has much lower requirements for radiometric sensitivity than a hyperspectral instrument. Very often, hyperspectral sensors are among the most sensitive solutions on the market of matrix optical sensors.

3. Digital image data processing

The digital-form of images, which enabled various ways of processing and presenting them had been, at the same time, the most important barrier in the first decades of the development of industrial and scientific vision systems. It was primarily related to the huge amount of data required for processing images acquired from two-dimensional matrices of CDD or CMOS sensors. While in the case of point measurement, its processing at a rate of hundreds of samples per second may be completely sufficient to automate such processes as, for example, control of temperature, position, and velocity of an object, in the case of an image this speed is many times too low. This is because images contain a relatively large amount of information, and even in today's highly digitally advanced world, systems for automatic image processing require correspondingly high computing power. Operations on millions of pixels require computing hardware at the level of at least a microcomputer. Analysis of massive volumes of data, especially in a real time, is challenging and requires application of sophisticated data processing. Recently, the application of deep learning methods seems to have been one of the solutions for an effective and proficient way of hypercube processing [40]. Nevertheless, key principles and process flow in most data processing schemes are the same as with the analytical approach – Fig. 1.

Hyper data cubes received from the imaging equipment in their raw form are full of artifacts, dead pixels, bad bands and redundant data. Removing or compressing these issues is the key goal of the first layer of the commonly used data processing scheme. In many cases operations

Metrol. Meas. Syst., Vol. 30 (2023), No. 4, pp. 637–654
DOI: 10.24425/mms.2023.147951

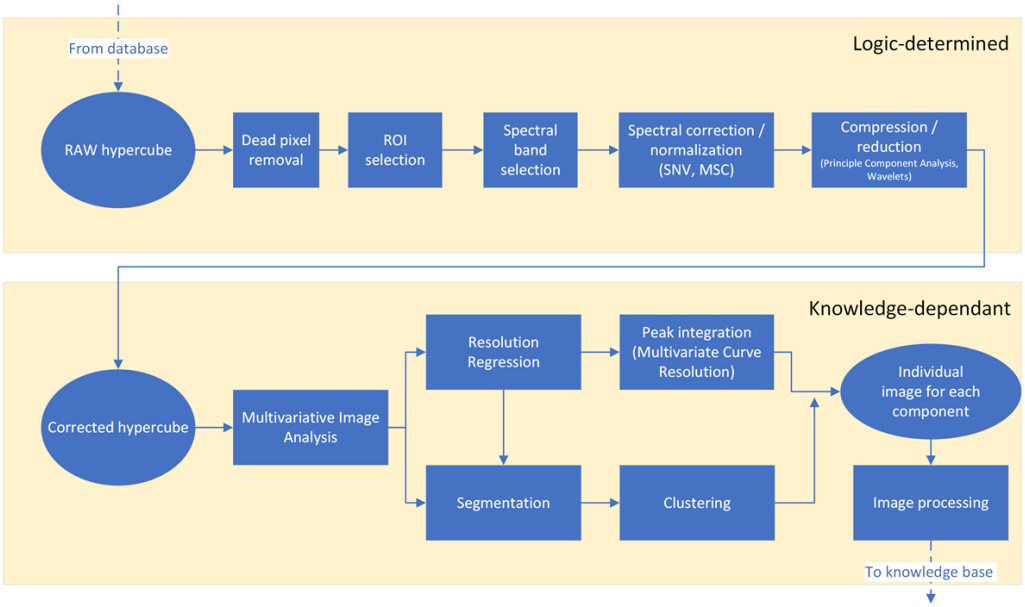

Fig. 1. Hypercube data processing scheme.

of this first layer are: dead pixel removal (based on sensor calibration data), ROI selection (or the selection of area to be processed), spectral band selection (based on application-related known correspondence between selected bands and the reflectance of objects of interest). Spectral correction is a tool for optimizing the reflectance range to the more comparable levels. There are several methods for such operations, the most common ones are SNV (*Standard Normal Variate*) and MSC (*Multiplicate Scatter Correction*). In many applications PCA (*Principal Component Analysis*) or Wavelet operations are the crucial next step. These operations are especially needed in high complexity hyperspectral data consisting of many spectral bands. The PCA or Wavelet approach reduce the number of spectral bands to only a fraction of initial raw data (for example from 150 bands to 6 bands). The bands are selected with the criterion of most valuable in the scope of distinguishable spectral signature features. After these pre-processing operations are completed, more complex tools are implemented, such as the Machine Learning approach. The steps of segmentation and clustering are the most dynamically developed operations, very often based on artificial intelligence (AI). Especially the combination and iterative approach to segmentation (often referred to as the re-representation of an image as a set of n one-band images instead of one n-band image) and clustering (which clusters similar pixels into regions classified as one type of object) are the subject of many interesting solutions, such as tree-based data partitioning structures [41]. This is due to the fact that after logically-determined first steps of hyperspectral image processing, segmentation and clustering are more challenging and knowledge or an application-dependent process is applied.

In this paper, the scheme of hyper data preprocessing is traced using an example of hyperspectral data collected by an airborne HYDICE instrument [42]. HYDICE was a push broom scanning, mechanically cooled, double-pass prism imaging spectrometer, placed on a C-141 aircraft pointing at nadir. It provided a wide spectrum of wavelengths from 0.4 µm to 2.5 µm, divided into two hundred, 10 nm-wide channels [43]. To this day, data from multiple imaging

campaigns provide high resolution hyperspectral imagery of urban and agricultural areas. Using one of the hypercubes provided by the HYDICE team [44], it is possible to develop and test new algorithms for hyperspectral data processing in urban area analysis applications. A preprocessing scheme, shown in this paper is one of the simplest and most effective approaches used by many researchers at early stages of data learning or familiarization with the data sets. It is also very narrow in scope (needing adjustments for every single use) and almost impossible to automate, since this approach requires human input on determination of fragments of the ground-truth set. Fig. 2 shows the visualization of a hypercube using spectral channels similar to what human eyesight perceives as red, green and blue colors.

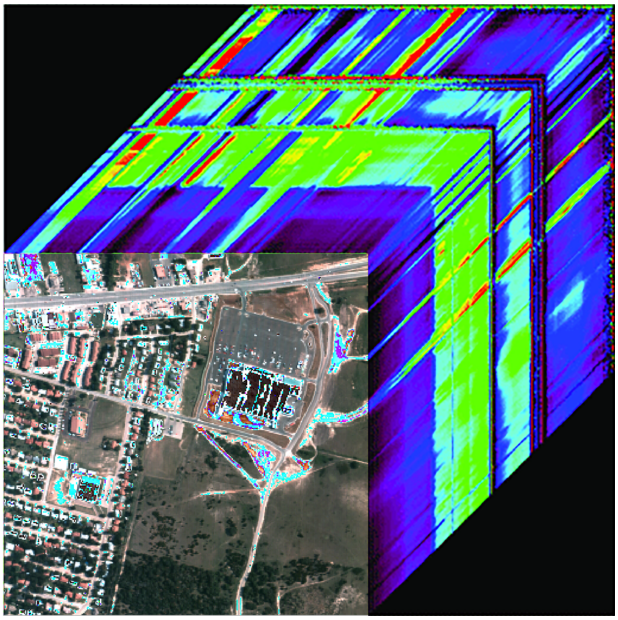

Fig. 2. Visualization of raw hypercube data from HYDICE.

In turn, Fig. 3 shows the subsequent steps of hypercube processing using the Spectronon [45] software with data gathered by HYDICE. One of the basic operations performed on spectral hypercubes is normalization because in raw hyperspectral data different objects can be registered as brighter than their environment due to their surface attitude (angle) between the light source and instrument. Because this implies an offset in the spectral data, if processed without normalization, the output data would be full of false object classification. The normalized plots shown in Fig. 3b are brought to standardized values throughout the spectral range. The resulting image, or more directly, its representation as an RGB image (Fig. 3a), still shows hardly distinguishable objects in the image and needs further processing. Standard Normal Variate and bad band removal are the next steps in the process. Fig. 3c shows the RGB image representation of the data, which shows much more distinguishable objects with a high definition of small buildings and differentiation in soil type. Fig. 3d confirms the proper removal of the bad band (compared to Fig. 3b). Such bad bands in the SWIR spectrum are corelated to atmospheric absorption of light due to water vapor and CO_2. The third important image is visualization presented in Fig. 3e, which is an RGB representation of the hypercube reduced to only 19 bands obtained by using the Principal Component Analysis. Three most interesting elements in the image for the urban application, *i.e.*

Metrol. Meas. Syst., Vol. 30 (2023), No. 4, pp. 637–654
DOI: 10.24425/mms.2023.147951

roof material, asphalt and grass or greens, are easily distinguishable by their reduced spectral plots seen in Fig. 3f. In the image, we can also see that objects of the same material, *e.g.* roads, are represented with the same color, which is a very good prognosis for further clustering.

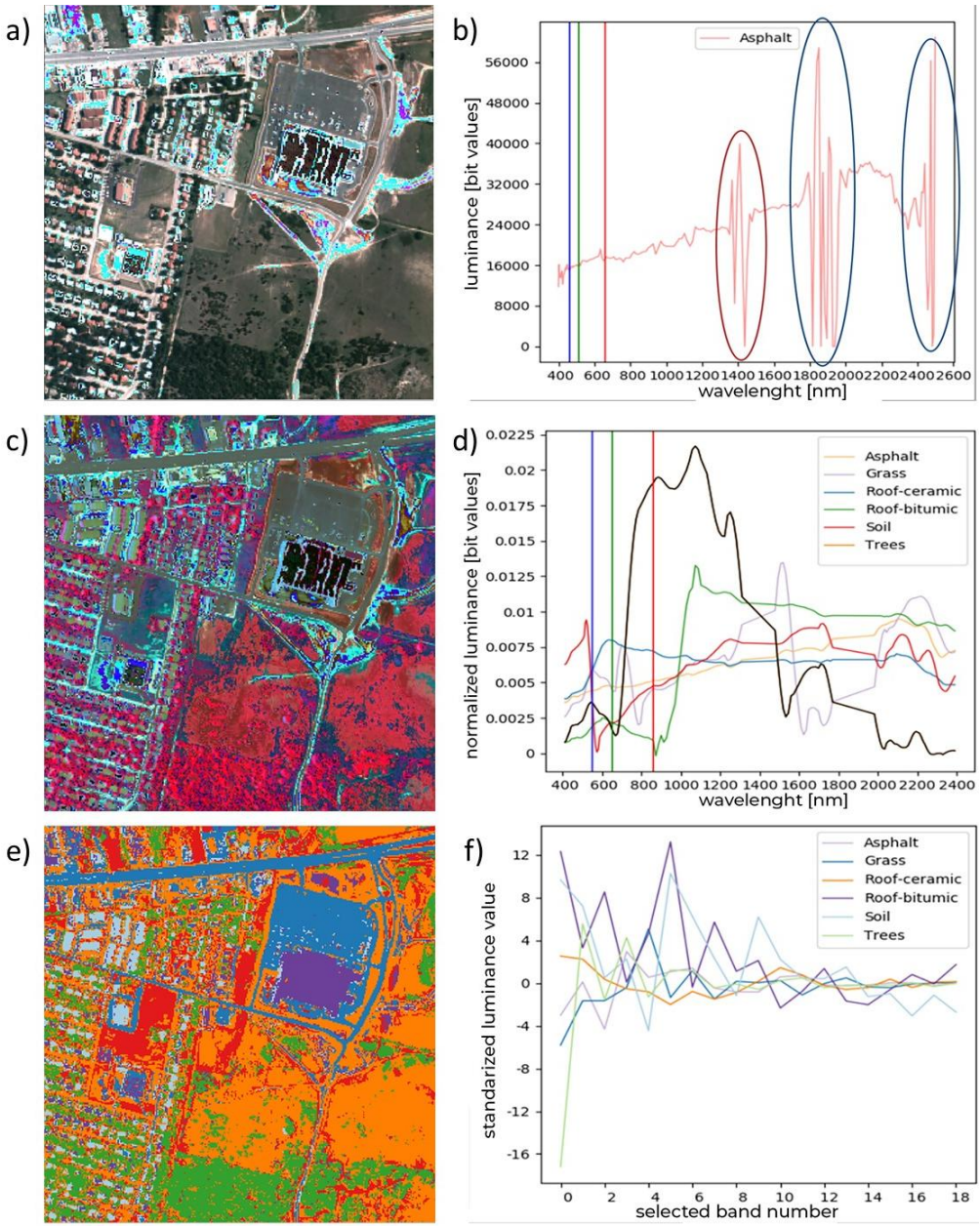

Fig. 3. Visualization of: a) normalized RGB data, b) mean spectrum plot (encircled bad channels caused by atmospheric water band blocking), c), RGB visualization of data after Standard Normal Variate correction, d), mean spectrum plot after SNV correction and bad band removal, e) RGB visualization of data with mean spectrum plot after Principal Component Analysis reduction to 19 key bands, f) spectral plots of materials in the image reduced to 19 key bands.

The classification of objects in the image can be obtained using different algorithms, such as, for example, k-Nearest neighbors. In Fig. 4, the result of such classification is shown as a map of abundance (indicated by white pixels) of classified objects. Fig. 4a shows regions with spectra similar to asphalt, Fig. 4b shows grass, and Fig. 4c shows roofs with ceramic surface. Fig. 4d shows the bitumic roof of a supermarket store. The last two Figures 4e and 4f represent spectra similar to soil and trees, respectively.

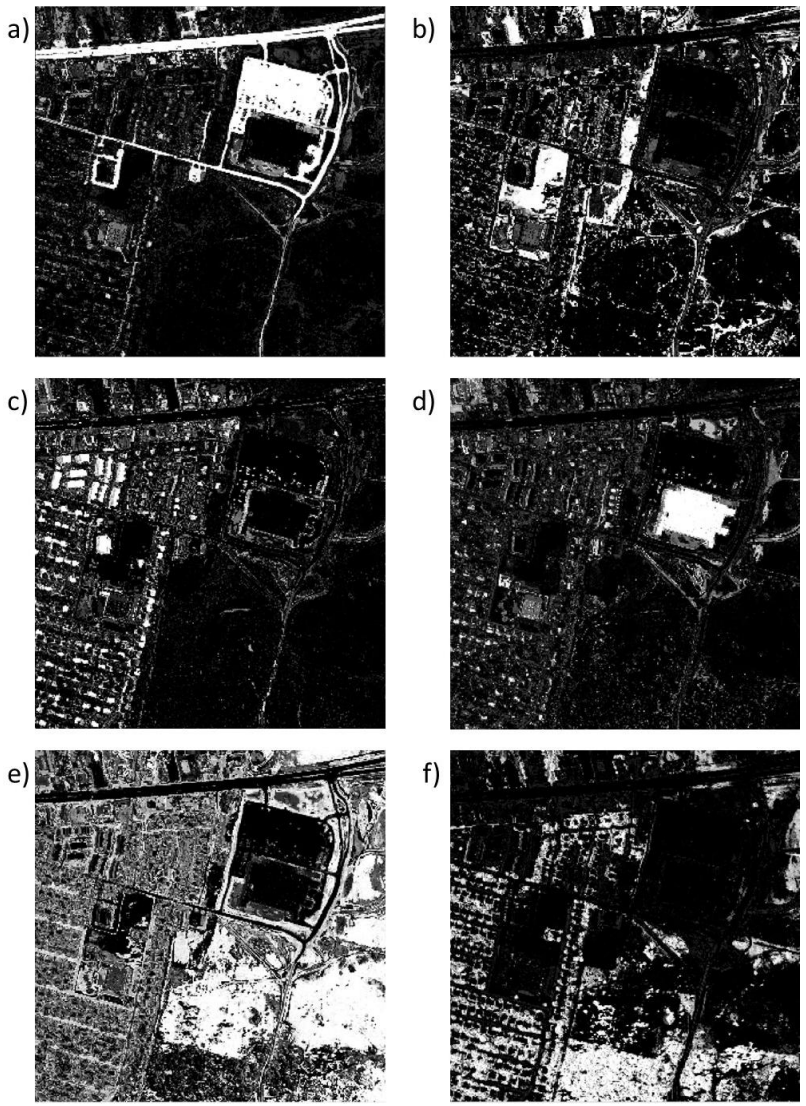

Fig. 4. Classification maps. White pixels indicate abundance of different classified materials: a) asphalt; b) grass; c) ceramic roofs; d) bitumic roofs; e) soil; f) trees.

The data used for this classification was generated manually, so individual spectra were pointed to the algorithm by hand. The novel approach to such data classification is based on the machine learning approach.

4. Recent achievements in the field of applications of spectral imaging

Nowadays, remote sensed hyperspectral data is mostly sourced from airplane platforms, UAVs and satellites [46], with strong commercial push toward orbital data. Historically, remote sensing campaigns collected considerable amounts of hyperspectral data, since the earlier mentioned 1966 airborne campaign performed by Michigan University of Technology. For almost 60 years, there have been many initiatives to establish as wide as possible hyperspectral datasets, and many research institutes, agencies, societies and even commercial data companies opened access to some of their data. Worth mentioning are datasets such as:

- Hyperspectral Salient Object Detection Dataset (HS-SOD) from National Institute of Advanced Industrial Science and Technology (Tokyo, Japan) [47],
- Indian Pines Hyperspectral Dataset from AVIRIS instrument available through the Purdue Research Foundation [48],
- Pavia Centre and University data acquired by an airborne ROSIS sensor and provided by the Telecommunications and Remote Sensing Laboratory [49],
- Kennedy Space Center data from AVRIS and opened by NASA [49],
- HYPER-VIEW soil dataset acquired by an UAV platform using a XIMEA camera, opened by KP Labs from Poland within the Hyperview Challenge [50–52].

Despite many selective datasets and more than a dozen orbital hyperspectral missions, currently hyperspectral data from satellites have not been yet easily accessible to downstream companies. This is slowly changing as various companies are planning to or have already sent their satellites (constellations) to space, such as Pixel, but it is very difficult to obtain any specific potential application for data processing from such companies. A literature review, however, reveals certain very interesting trends that can be described. However, one needs to filter the data as there are many publications and books that are considered as state-of-the-art, but they are simply outdated and cannot cover today's hyperspectral data.

Firstly, there is a huge push among the scientists to evaluate and create new, more efficient ways of processing any kind of hyperspectral data, regardless of the application. What is often mentioned is a data center needed to process the data, as it weighs more than the usual RGB image. Apart from the hypercube data processing, there have been many recent research projects or efforts which use modern data processing hardware – such as space-graded FPGAs to preprocess the data so that there is no need to download everything from the orbit. Another way to limit the number of pictures is to perform on-board classification of such data to see if it is usable. All those operations can be executed either by regular processing algorithms or by AI, which, in some of the cases, requires changes to the data processing process [53].

One of very promising applications of hyperspectral data, especially when considering climate change, is water quality monitoring from orbit, which can be performed in the way of detection of *e.g.* ammonia or different microorganisms. Hyperspectral data from orbit might be enhanced by airborne platforms that can provide more precise measurements with better resolution and revisit time.

Due to increasing popularity of hyperspectral imagers, more entities are looking towards integration of *e.g.* LIDAR or SAR data with hyperspectral images, which can provide very detailed information for agriculture industry. One of the examples of such data are individual plant species identification and 3D characterization at submeter scales. UAV LIDAR can characterize vegetation canopy and ground elevation, while hyperspectral data can allow to see what the dominant species on the ground is [54].

Hyperspectral data can be processed to obtain a product – information for customers – related to very specific and narrow markets, such as soybean, sugar cane farmers or vineyard owners. Such

services are provided by the Swiss company Gamay, which uses only UAVs for their business. In some cases, the customer is the government – NASA uses the Aviris imager to *e.g.* classify the ground after severe fires that happen from time to time in California.

Apart from the Earth Observation, there are also hyperspectral imagers that are developed for various applications that will help to establish human presence on the Moon. One of such case that is the use of a hyperspectral telescope or by very narrow spectral payload, is detection of certain minerals on the Moon to prepare places for future space mining operations [55].

5. Summary and future prospects

This paper presents a short review of hyperspectral imaging method illustrated with the authors' own example of HYDICE data processing. Recently, spectral imaging has been gaining new applications faster than ever before. This is connected mostly to broad accessibility of hyperspectral imagers and a much higher number of imaging campaigns from airborne and satellite platforms. Also, broader education in the field of image processing, AI and optoelectronics lead to much quicker development of hyperspectral analysis solutions. One of the examples of novel hyperspectral application is the detection of PM2.5 and PM10 particle concentration in air pollution measurements [56]. A research group from Taiwan elaborated on the use of hyperspectral cameras acquiring images in the visible and NIR ranges to map the poor air quality regions in urban regions. This method utilized key data processing steps such as brightness normalization and Principal Component Analysis, which resulted in very consistent measurements. What is worth noting is that, in the visible light approach, the correlation coefficients between the PM2.5 and PM10 measurements yielded a score of the 0.9789, which is a good indicator of usefulness of this method. Another, very meaningful example can be application of spectral imaging in agricultural disease control such as the detection of the 'orange rust' problem of sugarcane from the EO-1 Hyperion instrument [9]. Using the VNIR bands, it was possible to calculate spectral vegetation indices connected to leaf pigments, internal structure, and water content. Researchers have shown that, using discriminant function analysis, hyperspectral data can be used to determine regions of affected areas. Research also resulted in new vegetation indices, which are used in many problem detection applications in agriculture [9].

Acknowledgements

This paper was supported by the Ministry of Education and Science, Poland within the framework of the research project PhD Implementation, 5th Edition: "Methodologies for Acquisition, Processing and Analysis of Optical Hyperspectral Data in Industrial, Space, Mining and Agricultural Applications", (grant #DWD/5/0280/2021, 2021-2025).

References

[1] Barrett, H. H., & Myers, K. J. (2013). Foundations of image science. John Wiley & Sons.

[2] Manolakis, D. G., Lockwood, R. B., & Cooley, T. (2016). *Hyperspectral Imaging Remote Sensing: physics, sensors, and algorithms*. Cambridge University Press

[3] Qian, S-E (2020). *Hyperspectral Satellites and Systems Design*. CRC Press

[4] Zhang, W., & Zhao, L. (2022). The track, hotspot and frontier of international hyperspectral remote sensing research 2009–2019 – A bibliometric analysis based on SCI database. *Measurement*, *187*, 110229. https://doi.org/10.1016/j.measurement.2021.110229

[5] Huang, C., Tanaka T., Kagami, S., Ninomiya, Y., Kakuda, M., Watanabe, K., Inoue, S., Nanba, K., Igarashi, Y., Yamamoto, T., Shibuya, A., Nakahara, K., Arakawa, Y., & Yorozu, S. (2020). Multispectral imaging of mineral samples by infrared quantum dot focal plane array sensors. *Measurement*, *159*, 107775. https://doi.org/10.1016/j.measurement.2020.107775

[6] Pudełłko, A., Chodak, M., Roemer, J., & Uhl, T. (2020). Application of FT-NIR spectroscopy and NIR hyperspectral imaging to predict nitrogen and organic carbon contents in mine soils. *Measurement*, *164*, 108117. https://doi.org/10.1016/j.measurement.2020.108117

[7] Landgrebe, D. A. (2005). Multispectral land sensing: where from, where to? *IEEE Transactions on Geoscience and Remote Sensing*, *43*(3), 414–421. https://doi.org/10.1109/tgrs.2004.837327

[8] Goetz, A. F. H., & Srivastava, V. (1985). Mineralogical mapping in the Cuprite Mining District, Nevada. Proceedings of the Airborne Imaging Spectrometer Data Analysis Workshop (pp. 22–31). Pasadena, CA: JPL Publication 85–41.

[9] NASA. *Moderate Resolution Imaging Spectroradiometer*, Retrieved March, 2023, https://modis.gsfc.nasa.gov/about/specifications.php

[10] ESA. *Satellite Mission Catalogue, E)-1 (Earth Observing-1)*, eoPotral, Retrieved March, 2023, https://www.eoportal.org/satellite-missions/eo-1

[11] ESA. *Satellite Mission Catalogue, PROBA-1 (Project for On-Board Autonomy – 1)*, eoPotral, Retrieved March, 2023, https://www.eoportal.org/satellite-missions/proba-1

[12] ESA. *Satellite Mission Catalogue, ADEOS-II (Advanced Earth Observing Satellite-II) / Midori-II*, eoPotral, Retrieved March, 2023, https://www.eoportal.org/satellite-missions/adeos-ii

[13] ESA. *Satellite Mission Catalogue, IMS-1 (Indian Microsatellite-1)*, eoPotral, Retrieved March, 2023, https://www.eoportal.org/satellite-missions/ims-1

[14] ESA. *Satellite Mission Catalogue, HySIS (HyperSpectral Imaging Satellite)*, eoPotral, Retrieved March, 2023, https://www.eoportal.org/satellite-missions/hysis

[15] ESA. *Satellite Mission Catalogue, PRISMA (Hyperspectral)*, eoPotral, Retrieved March, 2023, https://www.eoportal.org/satellite-missions/prisma-hyperspectral

[16] ESA. *Satellite Mission Catalogue, Jilin Constellation*, eoPotral, Retrieved March, 2023, https://www.eoportal.org/satellite-missions/jilin-con

[17] ESA. *Satellite Mission Catalogue, ISS Utilization: HISUI (Hyperspectral Imager Suite)*, eoPotral, Retrieved March, 2023, https://www.eoportal.org/satellite-missions/iss-hisui

[18] ESA. *Satellite Mission Catalogue, GEO-KOMPSAT-2*, eoPotral, Retrieved March, 2023, https://www.eoportal.org/satellite-missions/geo-kompsat-2

[19] University of Twente. *EOS-3 (GISAT-1)*, Retrieved March, 2023, https://webapps.itc.utwente.nl/sensor/getsat.aspx?name=EOS-3%20(GISAT-1)

[20] ESA. *Satellite Mission Catalogue, EnMAP (Environmental Monitoring and Analysis Program)*, eoPotral, https://www.eoportal.org/satellite-missions/enmap

[21] Satellite Mission Catalogue, TEMPO (Tropospheric Emissions: Monitoring of Pollution), eoPotral, ESA, https://www.eoportal.org/satellite-missions/tempo

[22] Intuition-1 Mission, KP LABS, https://kplabs.space/intuition-1/

[23] Lee, C. M., Cable, M. L., Hook, S. J., Green, R. O., Ustin, S. L., Mandl, D., & Middleton, E. M. (2015). An introduction to the NASA Hyperspectral InfraRed Imager (HyspIRI) mission and preparatory activities. *Remote Sensing of Environment*, *167*, 6–19. https://doi.org/10.1016/j.rse.2015.06.012

[24] ESA. *Satellite Mission Catalogue, MetOp-SG (MetOp-Second Generation Program)*, eoPotral, Retrieved March, 2023, https://www.eoportal.org/satellite-missions/metop-sg

[25] Observing Systems Capability Analysis and Review Tool, World Meteorological Organization, MTG-S1, https://space.oscar.wmo.int/satellites/view/mtg_s1

[26] Corning (2017). *microHSI 410 SHARK Brochure*, https://www.corning.com/microsites/coc/oem/documents/hyperspectral-imaging/Corning-MicroHSI-410-SHARK-Brochure.pdf

[27] Cubert GmbH. *ULTRIS X20 PLUS*, Retrieved March, 2023, https://www.cubert-hyperspectral.com/products/ultris-x20-plus

[28] Eldim. *EZLITE HxS*, Retrieved March, 2023, https://eldim.biz/products/viewing-angle-multi-spectral/ezlite-hxs/

[29] EVK DI KERSCHHAGGL GMBH. *EVK HELIOS EQ32*, Retrieved March, 2023, https://www.evk.biz/en/products/hyperspectral-camera/evk-helios-eq32/

[30] Private communication

[31] HySpex. *Hyspex Cameras*. Retrieved March, 2023, https://www.hyspex.com/hyspex-products

[32] Imec, *Cameras*, Retrieved March, 2023, https://www.imechyperspectral.com/en/cameras

[33] Inno-Spec, Retrieved March, 2023, https://inno-spec.de/en/home-en-2/

[34] JAI, *FS-3200D-10GE*, Retrieved March, 2023, https://www.jai.com/products/fs-3200d-10ge

[35] LLA Instruments GmbH & Co. KG, *Analytical equipment for sorting machines in recycling*, Retrieved March, 2023, https://configurator.lla-instruments.de

[36] MicaSense, *RedEdge-MX Dual Camera System*, Retrieved March, 2023, https://support.micasense.com/hc/en-us/articles/360037369993-RedEdge-MX-Dual-Camera-System-Integration-Guide

[37] Ocean Insight, *FluxData*, Retrieved March, 2023, https://www.oceaninsight.com/fluxdata

[38] Specim, Retrieved March, 2023, https://www.specim.com/products/

[39] Isaza, C., Mosquera, J. M., Gómez-Méndez, G. A., Paz, Z. D., Jonny, P., Karina-Anaya, E., Rizzo-Sierra, J. A., & Palillero-Sandoval, O. (2019). Development of an acousto-optic system for hyperspectral image segmentation, *Metrology and Measurements Systems, 26*(3), 517–53. https://doi.org/10.24425/ mms.2019.129576

[40] Hilal, A. M., Al-Wesabi, F. N., Althobaiti, M. M., Al Duhayyim, M., Hamza, M. A., Kadry, S., & Rizwanullah, M. (2022). An Intelligent deep learning based hyperspectral Signal classification scheme for complex measurement systems. *Measurement*, *188*, 110540. https://doi.org/10.1016/j.measurement.2021.110540

[41] Ismail, M., & Orlandić, M. (2020). Segment-based clustering of hyperspectral images using tree-based data partitioning structures. *Algorithms*, *13*(12), 330. https://doi.org/10.3390/a13120330

[42] Index DataBase, *A database for remote sensing indices*. Retrieved March, 2023, https://www.indexdatabase.de/db/s-single.php?id=84

[43] Basedow, R., Silverglate, P., Rappoport, W., Rockwell, R., Rosenberg, D., Shu, K., Whittlesey, R., & Zalewski, E. (1993). The HYDICE Instrument Design and Its Application to Planetary Instruments, *Lunar and Planetary Inst., Workshop on Advanced Technologies for Planetary Instruments, Part 1*

[44] Geospatial Research Laboratory (U.S.). *HyperCube Sample Data Set: HYDICE sensor imagery URBAN*, Retrieved March, 2023, http://hdl.handle.net/11681/2925

[45] Resonon. Hyperspectral Software, Retrieved March, 2023, https://resonon.com/software

[46] Singh, S. (1999). Diffraction gratings: aberrations and applications. *Optics & Laser Technology*, *31*(3), 195–218. https://doi.org/10.1016/S0030-3992(99)00019-5

[47] Imamoglu, N., Oishi, Y., Zhang, X., Ding, G., Fang, Y., Kouyama, T., & Nakamura, R. (2018, May). Hyperspectral image dataset for benchmarking on salient object detection. In *2018 Tenth international conference on quality of multimedia experience (qoMEX)* (pp. 1–3). IEEE. https://doi.org/10.1109/QoMEX.2018.8463428

[48] Multispec. *A Freeware Multispectral Image Data Analysis System*, https://engineering.purdue.edu/~biehl/MultiSpec/hyperspectral.html

[49] Hyperspectral Remote Sensing Scenes, https://www.ehu.eus/ccwintco/index.php/Hyperspectral_Remote_Sensing_Scenes

[50] Seeing Beyond the Visible challenge, https://github.com/AI4EO/kp-labs-seeing-beyond-visible-challenge

[51] Nalepa, J., Saux, B. L., Longépé, N., Tulczyjew, L., Myller, M., Kawulok, M., Smykala, K., & Gumiela, M. (2022). The Hyperview Challenge: Estimating Soil Parameters from Hyperspectral Images. In *2022 IEEE International Conference on Image Processing (ICIP)*. https://doi.org/10.1109/icip46576.2022.9897443

[52] Kuzu, R. S., Albrecht, F., Arnold, C., Kamath, R., & Konen, K. (2022). Predicting Soil Properties from Hyperspectral Satellite Images. In *2022 IEEE International Conference on Image Processing (ICIP)*. https://doi.org/10.1109/icip46576.2022.9897254

[53] Hihara, H., Moritani, K., Inoue, M., Hoshi, Y., Iwasaki, A., Takada, J., Inada, H., Suzuki, M., Seki, T., Ichikawa, S., & Tanii, J. (2015). Onboard image processing system for hyperspectral sensor. *Sensors*, *15*(10), 24926–24944. https://doi.org/10.3390/s151024926

[54] Kahraman, S., & Bacher, R. (2021). A comprehensive review of hyperspectral data fusion with lidar and sar data. *Annual Reviews in Control*, *51*, 236–253. https://doi.org/10.1016/j.arcontrol.2021.03.003

[55] Sivakumar, V., Neelakantan, R., & Santosh, M. (2017). Lunar surface mineralogy using hyperspectral data: Implications for primordial crust in the Earth–Moon system. *Geoscience Frontiers*, *8*(3), 457–465. https://doi.org/10.1016/j.gsf.2016.03.005

[56] Chen, C., Tseng, Y., Mukundan, A., & Wang, H. (2021). Air pollution: Sensitive detection of PM2.5 and PM10 concentration using hyperspectral imaging. *Applied Sciences*, *11*(10), 4543. https://doi.org/10.3390/app11104543

Jędrzej Kowalewski received his M.Sc. degree in automation engineering from Wrocław University of Science and Technology. He is the founder and CEO of Scanway S.A., responsible for development and growth of the company. He has extensive experience in vision systems and hyperspectral imaging which he gathered while working at Wrocław University of Science and Technology and IWS Fraunhofer Dresden. He participated in one of the first Polish space projects implemented on the academia level, namely the FREDE and DREAM Projects and now he works as the R&D manager in most of Scanway's activities related to remote sensing and Earth Observation as well as in the field of hyperspectral imaging. He is pursuing his Ph.D. at Wrocław University of Science and Technology in which he focuses on hyperspectral data acquisition.

Michał Zięba received his M.Sc. Eng. degree in automation engineering from Wrocław University of Science and Technology. A former test engineer at one of the biggest automotive companies in Poland and a vision system specialist at one of the laboratories of Wrocław University of Science and Technology, at present he is the CTO at Scanway S.A. He participates in every major technical project implemented at Scanway, including those focused on hyperspectral imaging, realized for the space industry and manufacturing industries. He participated in the FREDE Project implemented with the European Space Agency at Wrocław University of Science and Technology.

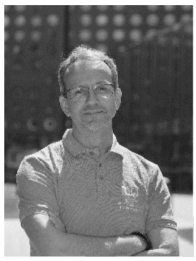

Jarosław Domaradzki is a full professor at the Faculty of Electronics, Photonics, and Microsystems at Wrocław University of Science and Technology, Poland. He received his M.Sc. degree in 1999, PhD in 2004 and D.Sc. degree in 2011. He received the title of full professor in 2020. His research interest is focused on technology and diagnostics of electrical and optical properties of thin films. His most important scientific achievements is the research that has led to the development of methods for modification and functionalization of thin-film coatings based on transparent oxide semiconductors. This achievement was preceded by development of several methods for the electrical and optical characterization, including imaging methods using a focused light beam.

Mikołaj Podgórski received his M.Sc. degree in power engineering and mechanical engineering from Wrocław University of Science and Technology. He is currently employed at Scanway S.A. where he works as the COO and manager of the space business unit. He is also the project manager of the biggest CEE Earth Observation space missions. He was one of the first to develop the Polish space sector through academia projects, implemented at Wrocław University of Science and Technology – including the FREDE and DREAM Projects. He has great expertise in the field of project management, business expansion, as well as systems engineering and resolving technical challenges. At the moment, he is pursuing his Ph.D. in the field of mechanical engineering with focus on systems engineering used in the development of space modules.